# Recent results from ultra-peripheral lead-lead collisions with ATLAS

K. Maj, on behalf of the ATLAS Collaboration[a]
*AGH University of Kraków*
*al. Mickiewicza 30, 30-059 Kraków, Poland*

Relativistic heavy-ion beams at the LHC are accompanied by a large flux of equivalent photons, leading to multiple photon-induced processes. This report presents a series of measurements of such processes performed by the ATLAS Collaboration. Measurements of exclusive dilepton production (electron, muon, and tau pairs) are discussed. These processes provide strong constraints on the nuclear photon flux and its dependence on the impact parameter and photon energy. In particular, measurements of the cross-sections in the presence of forward neutrons provide an additional experimental handle on the impact parameter range sampled in the observed events. Furthermore, the tau-pair production measurements can constrain the anomalous magnetic dipole moment of the tau lepton. High statistics measurements of light-by-light scattering shown in this talk provide a precise and unique opportunity to investigate extensions of the Standard Model, such as the presence of axion-like particles. The measurement of charged hadron in photonuclear collisions using 5.02 TeV Pb+Pb data collected in 2018 by ATLAS is also discussed. The charged hadron particle yields are presented as a functions of pseudorapidity and transverse momentum in different categories of event multiplicity. Measurement of jet production in ultra-peripheral collisions performed with the ATLAS detector using high-statistics 2018 Pb+Pb data is presented.

*Keywords:* ultra-peripheral collisions, photon-induced processes, exclusive dilepton production, anomalous magnetic moment, photonuclear dijet production, charged hadron, QGP

ATL-PHYS-PROC-2024-037
20 May 2024

## 1 Introduction

The ATLAS experiment [1] at the Large Hadron Collider (LHC) dedicates part of its annual operational time to the heavy-ion (HI) physics including ultra-peripheral collisions (UPC). The UPC are a unique category of HI collisions, which occur when the distance separating the interacting nuclei exceeds the sum of their radii. The large electromagnetic fields generated by relativistic ions can be considered as fluxes of photons - as described in the Equivalent Photon Approximation formalism [2,3]. Photon-induced interactions occur in both proton-proton, *pp*, and HI collisions. However, in the latter, the cross-sections for a specific process experience a significant increase due to the $Z^2$ scaling of the photon fluxes (where $Z$ is the atomic number). Furthermore, HI collisions exhibit minimal hadronic pile-up, allowing the identification of exclusive events and triggering on low-$p_{\mathrm{T}}$ particles. This exceptional characteristics make UPC an excellent tool for studying rare processes and searching for beyond Standard Model (BSM) phenomena, like axion-like particles in light-by-light ($\gamma\gamma \to \gamma\gamma$) scattering or setting constraints on the anomalous magnetic moment for the tau lepton using exclusive ditau production ($\gamma\gamma \to \tau^+\tau^-$). In the UPC events, photons provide a clean, energetic probe of the partonic structure of the nucleus, analogous to deep inelastic scattering. The photonuclear measurements are important for constraining the photon energy distribution and particle production in Monte Carlo (MC) models such as DPMJET-III [5]. Finally, the photon-induced processes offer a unique opportunity to probe the dynamics of Quantum Chromodynamics (QCD) in extremely asymmetric colliding systems, with energies between those available at RHIC and the LHC. Previous studies by the ATLAS experiment have revealed significant elliptic and triangular flow coefficients in the photonuclear events, indicating the presence of a quark-gluon plasma (QGP). Therefore, it becomes imperative to investigate these events for other potential QGP signatures, including radial flow, strangeness enhancement, and enhanced baryon/meson production.

This review presents the latest findings on ultra-peripheral Pb+Pb collisions from the ATLAS Collaboration. It examines photon-photon induced processes and jet production in UPCs using high-statistics 2018 Pb+Pb data. Additionally, it provides detailed insights into the properties of photonuclear collisions.

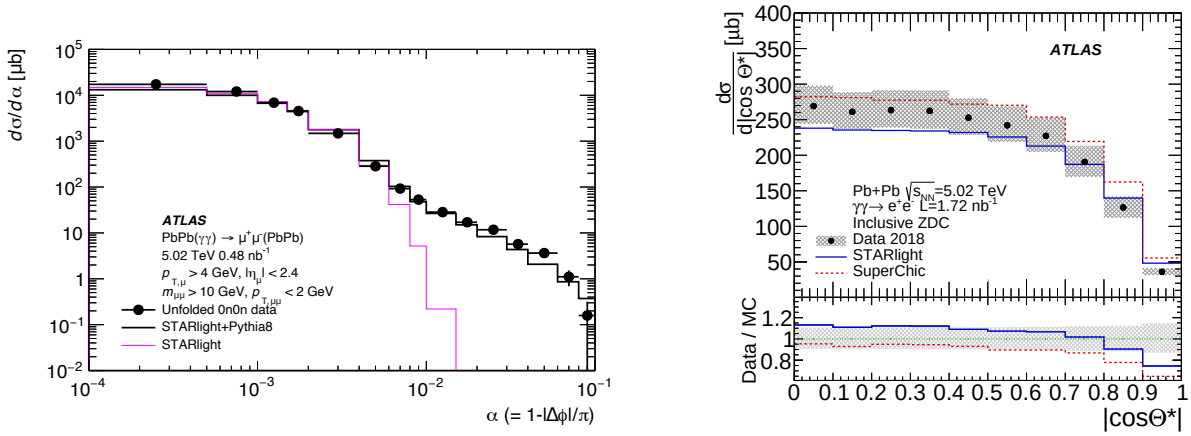


Figure 1: (Left) Differential cross-section as a function of acoplanarity for exclusive $\gamma\gamma \to \mu^+\mu^-$ production in UPC Pb+Pb collisions [6]. Data points are compared with predictions from STARlight and STARlight+PYTHIA8 to account for the FSR contribution. (Right) Differential cross-section measured as a function of $m_{ee}$ for exclusive dielectron production [9], $\gamma\gamma \to e^+e^-$. The bottom panel shows the ratio of the data and the predictions from STARlight and SuperChic.

.

## 2 Exclusive $\gamma\gamma \to \mu^+\mu^-$ and $\gamma\gamma \to e^+e^-$ production

ATLAS performed a measurement of exclusive $\gamma\gamma \to \mu^+\mu^-$ production [6] in UPC Pb+Pb collisions at $\sqrt{s_{\rm NN}} = 5.02$ TeV with an integrated luminosity of 0.48 nb$^{-1}$. The fiducial region of the measurement is defined with the final-state muons that are produced in azimuthal angle alignment and have low transverse momenta, $p_{\rm T} > 4$ GeV, and $|\eta| < 2.4$. Moreover, the dimuon mass, $m_{\mu\mu}$, has to be larger than 10 GeV, as well as, the $p_{\rm T}$ for the dimuon system, $p_{\rm T}^{\mu\mu}$, has to be below 2 GeV, to ensure a back-to-back topology. The event selection criteria ensure that each event contains exactly two oppositely charged muons with no additional activity in the detector. Dissociative background from nuclear break up is evaluated to be at the level of 3%.

The integrated fiducial cross-section for the exclusive dimuon production is measured to be: $\sigma = 34.1 \pm 0.3$ (stat.) $\pm 0.7$ (syst.) $\mu$b. The prediction from the STARlight [7] MC and STARlight+PYTHIA8 [8] MC are 32.1 $\mu$b and 30.8 $\mu$b, respectively, in agreement with the measurement. Differential cross-sections are measured as functions of several dimuon variables in the inclusive sample: $m_{\mu\mu}$, dimuon rapidity $y_{\mu\mu}$, scattering angle in the dimuon rest frame cosΘ*, initial-photon momenta $k_{\rm min}$, $k_{\rm max}$ and acoplanarity, $\alpha = 1 - \frac{|\Delta\phi|}{\pi}$. Figure 1 shows the differential cross section for exclusive $\gamma\gamma \to \mu^+\mu^-$ production as a function of $\alpha$. The predictions from STARlight and STARlight+PYTHIA8 are compared to the data. In general, a good agrement is found for both MC for $\alpha < 5 \times 10^{-3}$. For larger values of $\alpha$, the STARlight predictions underestimate the data. This discrepancy arises from the final state radiation (FSR), which is not included in the STARlight calculation. A more accurate representation of the complete $\alpha$ distribution is achieved by integrating STARlight with PYTHIA, which incorporates the FSR contribution.

Exclusive $\gamma\gamma \to e^+e^-$ production was measured [9] by the ATLAS experiment using 1.72 nb$^{-1}$ of Pb+Pb collision data at $\sqrt{s_{\rm NN}} = 5.02$ TeV collected in 2018. The evens exhibit characteristics similar to exclusive dimuon production, where two opposite-sign electrons with low transverse momentum are observed in a back-to-back configuration in the final state. The fiducial region, broader than that of the dimuon measurement, is defined by the following criteria: the electron $p_{\rm T} > 2.5$ GeV, $|\eta| < 2.5$, the dilectron mass ($m_{\rm ee}$) must be above 5 GeV, and the transverse momentum of the dielectron system ($p_{\rm T}^{ee}$) has to be below 2 GeV. A background contribution from dissociative production is estimated using the SuperChic [10] simulation normalised to the $\alpha$ data distribution.

The measured integrated fiducial cross-section for exclusive dielectron production is $\sigma = 215 \pm 1$ (stat.)$^{+23}_{-20}$ (syst.) $\pm 4$ (lumi.) $\mu$b. The predictions from STARlight and SuperChic are 196.9 $\mu$b and 235.1 $\mu$b, respectively, in agreement with the measurement. Differential cross-sections are determined as functions of multiple variables: $m_{ee}$, absolute dielectron rapidity, $|y_{ee}|$, average electron $p_{\rm T}$, $\langle p_{\rm T} \rangle$ and $|\cos\Theta^*|$. The latter is presented in the right panel of Figure 1. The precision of the measurement

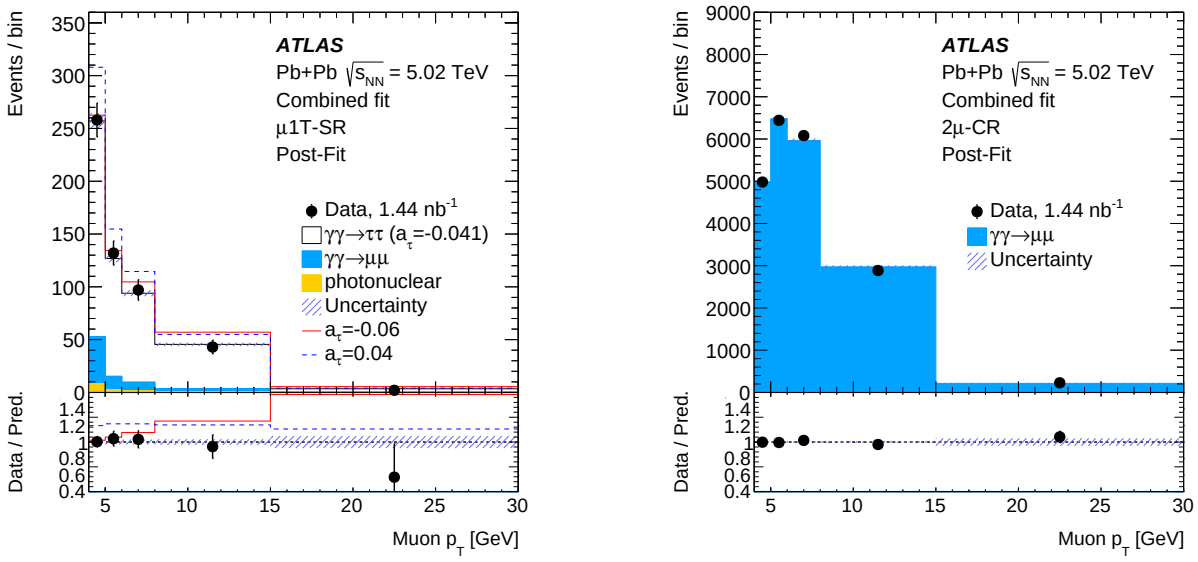


Figure 2: Muon $p_{\mathrm{T}}$ distributions in the (left) $\mu$1T-SR and (right) 2$\mu$-CR[11]. Post-fit distributions are shown with the signal contribution corresponding to the best-fit $a_\tau$ value ($a_\tau$=-0.042). For comparison, signal contributions with alternative $a_\tau$ values are shown.

is dominated by the systematic uncertainties. The MC predictions for the $\gamma\gamma \to e^+e^-$ process from STARlight and SuperChic are compared to the data. Both predictions underestimate or overestimate the data by about 10%. However, SuperChic tends to describe more accurately the shape of the distribution.

## 3 Exclusive $\gamma\gamma \to \tau^+\tau^-$ production and constraints on $a_\tau$

ATLAS provides the exclusive observation of $\gamma\gamma \to \tau^+\tau^-$ process [11] using data from 2018 Pb+Pb collisions at $\sqrt{s_{\mathrm{NN}}}$= 5.02 TeV with an integrated luminosity of 1.44 nb$^{-1}$. The measurement of the exclusive production of $\tau$-leptons is used to set new constraints on the anomalous magnetic moment of the $\tau$-lepton, $a_\tau$. The theoretical SM prediction is: $a_\tau^{\mathrm{SM}} = 0.00117721(5)$ [12], which is remarkably smaller than the currently available experimental bounds. Various BSM theories, such as lepton compositeness, supersymmetry, and TeV-scale leptoquarks, etc., predicted modifications to the SM value of $a_\tau$. The most stringent limits on $a_\tau$ are currently provided by the DELPHI experiment: $-0.052 < a_\tau < 0.013$ (95% CL) [13].

The identification techniques commonly employed in ATLAS cannot be used for signal $\tau$-leptons due to its very low $p_{\mathrm{T}}$ values. Instead, it is required that events considered in the analysis contain one muon from the decay of one of the $\tau$-leptons, and an electron or charged-particle track(s) from the decay of the other $\tau$-lepton. Three distinct signal regions (SR) are defined: muon and electron ($\mu e$-SR), muon and one track ($\mu$1T-SR), and muon and three tracks ($\mu$3T-SR). Candidate events are selected with a single muon trigger requiring muon $p_{\mathrm{T}}$ above 4 GeV. To ensure the exclusivity of the selected events, a veto on forward neutron activity in the Zero Degree Calorimeter (ZDC) is imposed. Muons selected for the analysis are required to have $p_{\mathrm{T}} > 4$ GeV and $|\eta| < 2.4$, selected electrons have $p_{\mathrm{T}} > 4$ GeV and $|\eta| < 2.47$ and selected tracks should have $p_{\mathrm{T}} > 100$ MeV and $|\eta| < 2.5$. Events containing additional low-$p_{\mathrm{T}}$ tracks are rejected. Since different background processes contribute to each signal category, further requirements are introduced in the $\mu$1T-SR (muon and track system $p_{\mathrm{T}} > 1$ GeV) and the $\mu$3T-SR (mass of the three-track system below 1.7 GeV). The main sources of background contributions arise from the exclusive dimuon production with the final-state radiation (FSR) and diffractive photonuclear interactions. The $\gamma\gamma \to \mu\mu$ background is constrained with a dimuon control region, 2$\mu$-CR. It requires exactly two opposite-charge muons with invariant mass above 11 GeV to suppress quarkonia backgrounds and no additional tracks separated from the muons by $\Delta R_{\mu,\mathrm{trk}} > 0.1$.

After applying the event selection, a total of 656 data events were observed in the three signal regions in which the analysis was performed. To measure $a_\tau$, a fit to the muon $p_{\mathrm{T}}$ distribution is performed in the three SRs with $a_\tau$ being the parameter of interest. Also a control region with events from the $\gamma\gamma \to \mu^+\mu^-$ process is used in the fit to constrain initial-photon fluxes. The fitted muon $p_{\mathrm{T}}$ distributions

for the $\mu$1T-SR and 2$\mu$-CR are shown in Figure 2. A very good data-to-prediction agreement is seen for the best-fit value of the $a_\tau$. The $\gamma\gamma \to \tau^+\tau^-$ process was observed with a significance exceeding 5 standard deviations, and a signal strength of $\mu_{\tau\tau} = 1.03^{+0.06}_{-0.05}$ assuming the SM value of $a_\tau$. Figure 3 presents a comparison of the ATLAS measurement of the anomalous magnetic moment of the $\tau$-lepton and previous results obtained at the LEP experiments. The precision of this measurement is similar to the most precise single-experiment measurement by the DELPHI Collaboration [13].

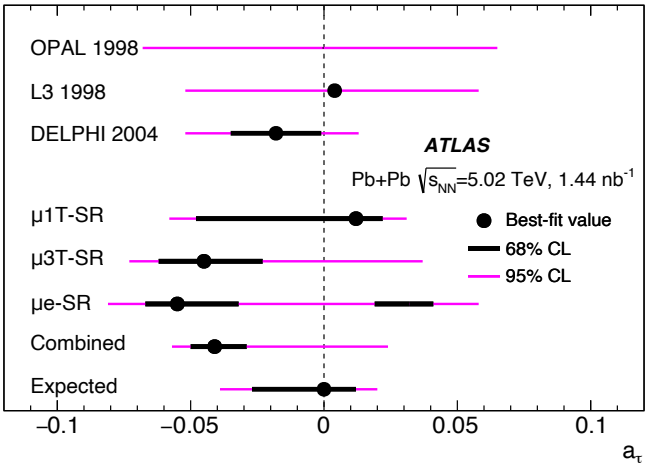


Figure 3: Measurements of $a_\tau$ from fits to individual signal regions (including the 2$\mu$-CR), and from the combined fit [11]. Measurements from the OPAL [14], L3 [15] and DELPHI [13] experiments at LEP are also included for comparison.

## 4 Light-by-light scattering and search for axion-like particles

The light-by-light ($\gamma\gamma \to \gamma\gamma$, LbyL) scattering is a rare phenomenon which proceed via quantum electrodynamics (QED) at the lowest order via a loop of virtual charged fermions or $W^\pm$ bosons. LbyL production can be altered by various BSM phenomena: new particles entering the loop, Born-Infeld extensions of QED, space-time non-commutativity in QED, extra spatial dimensions, etc. Furthermore, the diphoton mass spectrum obtained from the LbyL process can be explored to search for potential neutral axion-like particles, ALP. ALP may contribute to the distribution as a narrow diphoton resonance [16].

LbyL scattering was also measured [17] by ATLAS in UPC Pb+Pb collisions at $\sqrt{s_{\rm NN}} = 5.02$ TeV using a combined 2015+2018 data sample with an integrated luminosity of 2.2 nb$^{-1}$. The signature of interest is the exclusive production of two photons, each with transverse energy $E_{\rm T}^\gamma > 2.5$ GeV, pseudorapidity $|\eta^\gamma| < 2.4$ and diphoton invariant mass $m_{\gamma\gamma} > 5$ GeV with transverse momentum $p_{\rm T}^{\gamma\gamma} < 1$ GeV. Any extra activity in the detector is vetoed, in particular no reconstructed tracks originating from the nominal interaction point with $p_{\rm T} > 100$ MeV are accepted. The final state photons are aligned in the azimuthal angle $\phi$. Back-to-back topology is studied using diphoton acoplanarity, defined as $A_\phi = 1 - \frac{|\Delta\phi|}{\pi}$. Event candidates are expected to have $A_\phi < 0.01$. The main background contribution originates from exclusive production of the electron–positron pairs ($\gamma\gamma \to e^+e^-$). In the measurement, the $\gamma\gamma \to e^+e^-$ background is suppressed with the requirement of no tracks and pixel-tracks reconstructed in the Inner Detector. A remaining dielectron contribution is evaluated using a data-driven method. The second significant background source is gluon-induced central exclusive production (CEP) of photon pairs. The CEP background is evaluated using a dedicated control region in data ($A_\phi > 0.01$) and then extrapolated to the LbyL signal region.

ATLAS established the observation of the LbyL process with 97 events observed in data, while the signal and background expectations are 45 events and 27 $\pm$ 5 events, respectively. The integrated cross-section measured in the fiducial phase space, defined by requirements reflecting the event selection, is $\sigma_{fid} = 120 \pm 17$ (stat.) $\pm 13$ (syst.) $\pm 4$ (lumi) nb. The predictions from the SuperChic v3.0 [18] and from Ref.[19] are 78$\pm$ 8 and 80 $\pm$ 8 nb, respectively. In addition to the integrated fiducial cross-section, ATLAS measured $\gamma\gamma \to \gamma\gamma$ differential cross-sections involving four kinematic variables of the final-state photons. In general, a good agreement between the measurement and SM predictions is found.

ALP may be produced in the photon–photon fusion, $\gamma\gamma \to a \to \gamma\gamma$, followed by the decay to the diphoton pair, where $a$ denotes the ALP field. Thus, a diphoton invariant mass distribution, $m_{\gamma\gamma}$,

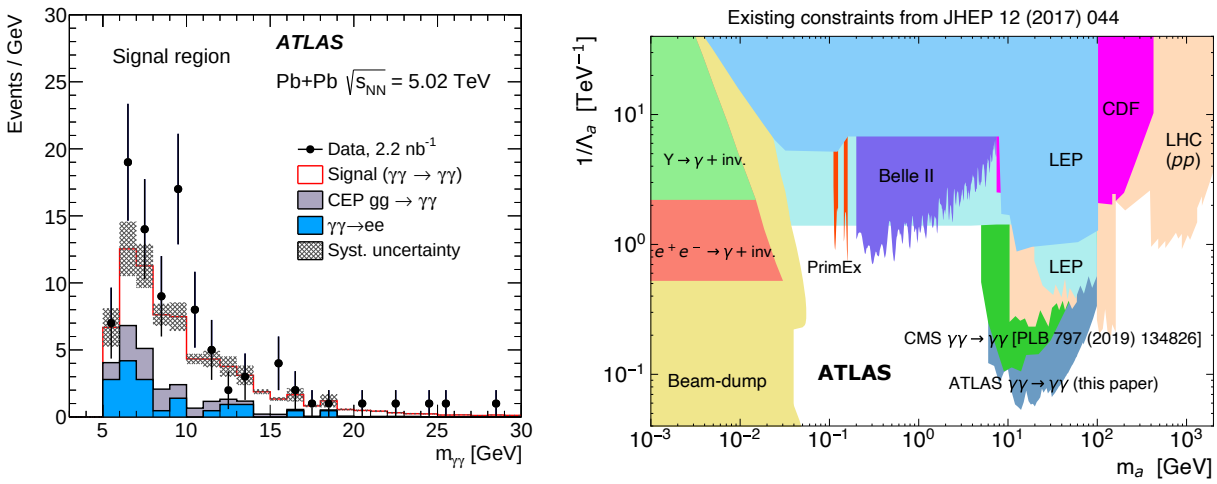


Figure 4: (Left) The diphoton invariant mass for $\gamma\gamma \to \gamma\gamma$ event candidates [17]. The sum of the signal and background expectations are compared to the data. (Right) Compilation of exclusion limits at 95% CL in the ALP-photon coupling ($1/\Lambda_a$) versus ALP mass ($m_a$) plane obtained by different experiments. The new limit obtained by ATLAS is marked with the label: ATLAS $\gamma\gamma \to \gamma\gamma$ [17]

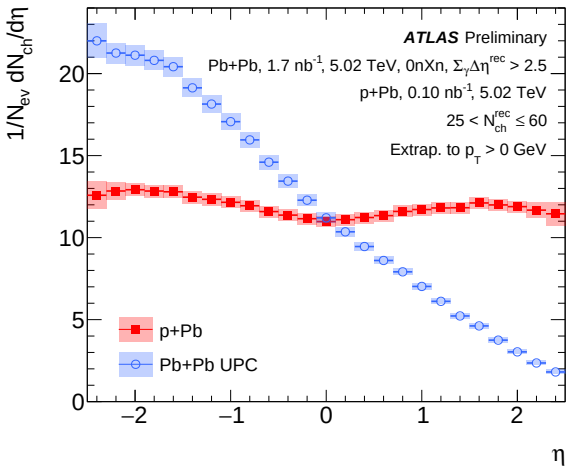


Figure 5: The charged-hadron yields as a function of $\eta$ extrapolated to $p_{\mathrm{T}} > 0$ GeV for Pb+Pb UPC and p+Pb collisions [23].

presented in the left panel of Figure 4, can be used for ALP searches. The ALP production would result in a resonance peak with diphoton mass equal to the mass of $a$. The diphoton mass distribution was examined for a mass range between 6 and 100 GeV. No significant excess of events over expected background was found in the analysis. The 95% CL limit was derived for ALP production cross-section and ALP coupling to photons $\frac{1}{\Lambda_a}$ as a function of ALP mass. A summary of the exclusion limits from different experiments together with the new ATLAS constraints is shown in the right panel of Figure 4.

## 5 Charged hadrons yield measurements in photonuclear events

QGP matter is typically discussed in terms of head-on heavy-ion collisions. However, QGP-like signals have been also observed in smaller systems such as p+Pb, pp, or d+Au. Photons associated with nuclei can break apart the other colliding nuclei, resulting in photon-nucleus or photon-photon interactions. ATLAS measured two-particle azimuthal correlations in the photonuclear events, revealing significant non-zero elliptic ($v_2$) and triangular ($v_3$) flow coefficients [20]. The results can be interpreted as indication of a hydrodynamically flowing medium. In Ref. [21], the authors predict that radial flow [22], a signature for

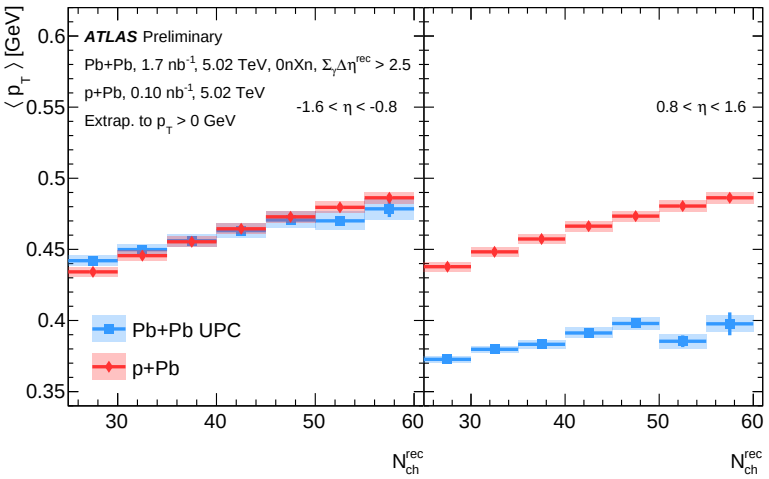


Figure 6: The $\langle p_{\mathrm{T}} \rangle$ of charged-hadron yields as a function of $\mathrm{N}_{\mathrm{ch}}^{\mathrm{rec}}$ in Pb+Pb UPC collisions and p+Pb collisions [23] for $-1.6 < \eta < -0.8$ (left) and $0.8 < \eta < 1.6$ (right). The charged-hadron yields are extrapolated to $p_{\mathrm{T}} > 0$ GeV.

QGP, should be essentially the same in UPC and p+Pb collisions. This can be measured via the mean transverse momentum $\langle p_{\mathrm{T}} \rangle$ of charged and identified particles. To test this prediction, ATLAS performed measurement [23] of inclusive yields of primary charged hadrons as functions of $\eta$, $p_{\mathrm{T}}$ and in selections of charge particle multiplicity $N_{\mathrm{ch}}^{\mathrm{rec}}$ in Pb+Pb UPC and p+Pb collisions.

The charged-hadron yields in Pb+Pb UPC and p+Pb collisions integrated over $p_{\mathrm{T}}$ as a function of $\eta$ are shown in Figure 5. Negative $\eta$ corresponds to the direction of the lead nucleus (Pb-going), while positive $\eta$ corresponds to the direction of the photon (photon-going) and the proton (proton-going) in Pb+Pb and p+Pb collisions, respectively. The distribution in Pb+Pb UPC is highly asymmetric due to the lower energy of the photon compared to the energy per nucleon in the opposing lead nucleus.

Figure 6 shows $\langle p_{\mathrm{T}} \rangle$ for $p_{\mathrm{T}} > 0$ GeV as a function of $\mathrm{N}_{\mathrm{ch}}^{\mathrm{rec}}$ in two $\eta$ regions, [-1.6,-0.8] and [0.8,1.6], in Pb+Pb UPC and p+Pb collisions. At negative $\eta$, $\langle p_{\mathrm{T}} \rangle$ between the two collision systems is comparable. In contrast, on the photon-going side ($\eta > 0$), there is a large difference in the $\langle p_{\mathrm{T}} \rangle$ between the two collision systems for all $\mathrm{N}_{\mathrm{ch}}^{\mathrm{rec}}$. The substantially larger $\mathrm{N}_{\mathrm{ch}}^{\mathrm{rec}}$ at negative $\eta$ in Pb+Pb UPC and its comparable magnitude in p+Pb may suggest a contribution from radial flow. Further tests measuring the $\langle p_{\mathrm{T}} \rangle$ of identified hadrons are needed to confirm this hypothesis.

## 6 Photonuclear jet production

ATLAS also performed the measurement of di-jet photoproduction in ultra-peripheral Pb+Pb collisions [24]. The measurement uses data recorded in 2018 with an integrated luminosity of 1.72 $\mathrm{nb}^{-1}$. Photonuclear events are selected using a combination of ZDC and rapidity gap requirements. In particular, events are required to satisfy only a 0nXn condition that requires no neutrons in the photon-going direction and one or more neutrons in the other direction. The jets are reconstructed from particle-flow inputs using the anti-$k_{\mathrm{t}}$ algorithm [25] with R = 0.4. Figure 7 shows the triple-differential cross-sections as a function of the photon parton momentum fraction, $z_\gamma$ (left), the nuclear parton momentum fraction, $x_{\mathrm{A}}$, (right) both cross-sections are presented in different regions of the jet transverse momenta, $H_{\mathrm{T}}$. The $z_\gamma$ dependence over a narrow $x_{\mathrm{A}}$ interval should be determined, primarily, by the photon flux. Thus, results like these should provide an important constraint on theoretical calculations of both the flux and the breakup probability for the photon-emitting nucleus.

## 7 Summary

This report presents the latest findings on ultra-peripheral Pb+Pb collisions from the ATLAS Collaboration, focusing on photon-photon induced processes and jet production using high-statistics 2018 Pb+Pb data. It also provides detailed insights into the properties of photonuclear collisions. The exclusive $e^+e^-$ and $\mu^+\mu^-$ productions were measured by the ATLAS experiment using UPC data at $\sqrt{s_{\mathrm{NN}}} = 5.02$

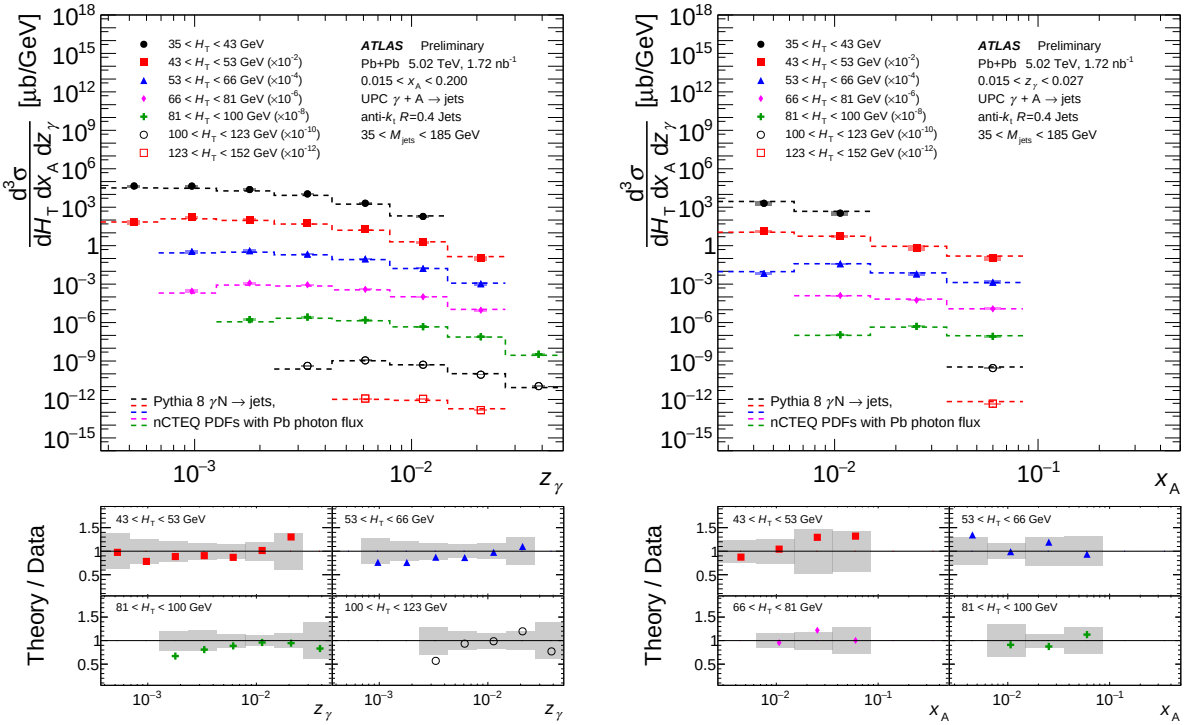


Figure 7: (Left) Triple-differential cross-sections [24], $\mathrm{d}^3\sigma/\mathrm{d}H_T\mathrm{d}x_A\mathrm{d}z_\gamma$, as functions of $z_\gamma$ for different bins of $H_T$ for events with struck parton energies in the kinematic range $0.015 < x_A < 0.2$. (Right) The same cross-sections as a functions of $x_A$ for different bins of $H_T$ for events with emitted photon energies in the kinematic range $0.015 < z_\gamma < 0.027$.

TeV. The theory predictions from STARlight and SuperChic were compared to the measured fiducial cross-sections and show discrepancies at the level of several percent, with STARlight (SuperChic) underestimating (overestimating) the data. The results of the differential cross-sections provide a reference for other photon-induced processes and for various theoretical approaches to model the photon fluxes. The $\gamma\gamma \to \tau^+\tau^-$ process has been observed in Pb+Pb UPC by the ATLAS experiment, surpassing a $5\sigma$ significance. The signal strength is consistent with the Standard Model expectations. The new constraints on the $a_\tau$ have been set, and are competitive to the best limits obtained during the LEP era. With the upcoming Run-3 data, an improvement in precision is anticipated. Additionally, the ATLAS experiment has established the presence of $\gamma\gamma \to \gamma\gamma$ scattering, with the results consistent with the Standard Model prediction. The measured invariant mass of the diphoton system was used to set new exclusion limits on axion-like particles. Charged-hadron yields were quantified in UPC photonuclear interactions by ATLAS. Also the mean $p_\mathrm{T}$ value of yields measured in $\eta$ intervals, were measured within selections of $\mathrm{N}_\mathrm{ch}^\mathrm{rec}$. Potential signatures of collectivity including radial expansion were tested via the $\langle p_\mathrm{T}\rangle$ comparison in Pb+Pb UPC and p+Pb collisions. The larger $\langle p_\mathrm{T}\rangle$ at backward compared to forward rapidity in Pb+Pb UPC may suggest the presence of hydrodynamic radial flow. Finally the measurement of the triple-differential cross-section for photonnuclear events were discussed. These results provide an important step towards the goal of a precise limit on nuclear PDFs in this region by quantifying theoretical components, such as the electromagnetic breakup fraction, which are necessary for a precise comparison to theory.

## Acknowledgments

This work was partly supported by program "Excellence initiative – research university" for the AGH University of Kraków and by the National Science Centre of Poland under grant number UMO-2021/40/C/ST2/00187.

## References

1. ATLAS Collaboration, JINST **3**, (2008) S08003.

2. E. Fermi, Nuovo Cim **2**, (1925) 143.
3. E. J. Williams, Phys. Rev. Journals Archive **45**, (1934) 729.
4. R. Engel, Z. Phys. C **66**, (1995) 203.
5. S. Roesler et al., Advanced Monte Carlo for Radiation Physics, arXiv: hep-ph/0012252, (2001).
6. ATLAS Collaboration, Phys. Rev. **C 104**, (2021) 024906.
7. S.R. Klein et al., Comp. Phys. Comm. **212**, (2017) 258.
8. T. Sjostrand et al., Comp. Phys. Comm. **191**, (2015) 159.
9. ATLAS Collaboration, J. High Energy Phys. **06**, (2023) 182.
10. L. A. Harland-Lang et al., Eur. Phys. J. C **76**, (2016) 9.
11. ATLAS Collaboration, Phys. Rev. Lett. **131**, (2023) 151802.
12. S. Eidelman, and M. Passera, Mod. Phys. Lett. A **22**, (2007) 159.
13. J. Abdallah et al., DELPHI Collaboration, Eur. Phys. J. C **35**, (2004) 159.
14. OPAL Collaboration, Phys. Lett. B **431**, (1998) 188.
15. L3 Collaboration, Phys. Lett. B **434**, (1998) 169.
16. S. Knapen, T. T. Lin, H. K. Lou and T. Melia, Phys. Rev. Lett. **118**, (2017) 171801.
17. ATLAS Collaboration, J. High Energy Phys. **3**, (2021) 243.
18. L. A. Harland-Lang et al., Eur. Phys. J. C **79**, (2019) 39.
19. M. Kłusek-Gawenda et al., Phys. Rev. C **93**, (2016) 044907.
20. ATLAS Collaboration Phys. Rev. C **104** (2021) 014903.
21. W. Zhao et al., Phys. Rev. Lett. **129**, (2022) 252302.
22. U. Heinz, R. Snellings, Ann. Rev. Nucl. Part. Sci. **63**, (2013) 123.
23. ATLAS Collaboration, ATLAS-CONF-2023-059, https://cds.cern.ch/record/2871729 (2023).
24. ATLAS Collaboration ATLAS-CONF-2022-021 https://cds.cern.ch/record/2806461 (2022).
25. M. Cacciari et al., J. High Energy Phys. **04**, (2008) 063.